Applied Catalysis B: Environmental 117–118 (2012) 310–316

Contents lists available at SciVerse ScienceDirect

Applied Catalysis B: Environmental

journal homepage: www.elsevier.com/locate/apcatb

Iron–sulfur codoped TiO_2 anatase nano-materials: UV and sunlight activity for toluene degradation

Konstantinos C. Christoforidis[a], Santiago J.A. Figueroa[b], Marcos Fernández-García[a,*]

[a] Instituto de Catálisis y Petroleoquímica, CSIC, C/Marie Curie 2, Cantoblanco, 28049-Madrid, Spain
[b] European Synchrotron Radiation Facility, R/Jules Horowitz 6, BP220, F-38043 Grenoble, France

ARTICLE INFO

Article history:
Received 12 December 2011
Received in revised form 19 January 2012
Accepted 24 January 2012
Available online 1 February 2012

Keywords:
Photocatalysis
Titania
Anatase
Iron
Fe
Sulfur
Co-doping
Selective partial oxidation
Toluene
Benzaldehyde

ABSTRACT

Iron and sulfur single- and co-doped TiO_2 nanocrystals were prepared and characterized by a multitechnique approach. The presence of sulfur affected drastically the crystal size of anatase as well as other morphological characteristics such as BET surface area, pore volume and pore size. Significant differences were also detected on the isolated OH species concentration as a function of sulfur content. On the contrary, X-ray absorption spectroscopy (XAFS) showed that sulfur did not alter substantially the structural and electronic properties of Fe on TiO_2. The photocatalytic activity of the synthesized TiO_2 powders was studied in the gas-phase oxidation of toluene. The trials showed that the co-doped S/Fe-TiO_2 nanomaterials have enhanced photo-activity compared to the reference single-doped Fe-TiO_2 under both sunlight and UV-light irradiation. This is not however the case if compared with the single S-doped materials. Sulfur additionally modifies the selectivity of toluene photo-oxidation toward partial oxidation products. The partial vs. total oxidation yield ratio increased with increasing S content in both co-doped S/Fe-TiO_2 or single-doped S-TiO_2 series and was attributed to differences in surface properties related to both S-containing and OH entities.

1. Introduction

Nanostructured titanium dioxide (TiO_2) has been widely used as photocatalyst for environmental cleanup mainly due to its low cost and physicochemical properties (high thermal and chemical stability, low toxicity, relatively high photocatalytic activity) [1]. However, due to its UV-driven photocatalytic activity caused by its wide bandgap (≈3.2 eV for anatase), its application under sunlight irradiation is limited. Hence, the improvement and optimization of TiO_2 as photocatalyst under solar-light irradiation is of great importance. Toward this objective, intensive efforts have been driven to the introduction of dopants into TiO_2 lattice.

Various dopants have been applied including transition metal ions (i.e. Fe, Co, Cu) as well as nonmetal dopants (i.e. N, C, S, F). Doping of transition metals has been largely employed in order to enhance the photocatalytic activity of TiO_2. Metal-doped TiO_2 has been shown to induce the desired red-shift of the adsorption spectrum. However, it has also been documented that the presence of transition metals may increase the probability of electron–hole recombination, reducing in this way the semiconductor's photocatalytic efficiency [2,3]. Iron(III) is one of the most frequently examined dopants [1,2,4,5] due to the fact the radius of Fe^{3+} (0.79 Å) is similar to that of Ti^{4+} (0.75 Å), and hence it can be easily incorporated into the crystal lattice of TiO_2 [6,7]. However, the role of Fe ions in TiO_2 is controversial. It has been suggested that Fe^{3+} behaves as electron–hole recombination center, inhibiting the photo-activity [8] or favors electron–hole separation, enhancing the photo-activity [7,9–12].

Titania doping with nonmetal elements has been also considered as an effective approach to extend the spectral response of TiO_2 toward to lower energy wavelengths. In this approach, sulfur doped TiO_2 catalysts have been reported to exhibit enhanced photocatalytic activity under visible light irradiation [13–16]. Recently, emphasis has been given on codoped titania systems, involving cations and anions, in order to improve the photocatalytic efficiency of TiO_2 [17–21]. Concerning Fe and S codoped materials, it has been proposed that charge separation between electrons and holes is improved [22,23].

The present work outlines the preparation of a series of Fe,S single- and co-doped anatase titania prepared by chemically modifying titanium isopropoxide precursor using the microemulsion procedure. A multitechnique approach (UV-Vis, N_2 isotherms, DRIFT, XRD, XANES) was used to study the structural and electronic

* Corresponding author. Tel.: +34 915 85 49 39; fax: +34 915 85 47 60.
E-mail addresses: christoforidis.k@icp.csic.es (K.C. Christoforidis), m.fernandez@icp.csic.es, mfg@icp.csic.es (M. Fernández-García).

0926-3373/$ – see front matter © 2012 Elsevier B.V. All rights reserved.
doi:10.1016/j.apcatb.2012.01.029

properties of the prepared catalysts. The catalysts were evaluated against sunlight and UV-light gas-phase photo-oxidation of toluene including their selectivity concerning total and partial oxidized products.

2. Experimental

2.1. Catalyst preparation

Titania precursor materials were prepared using a microemulsion synthetic route by the addition of titanium(IV) isopropoxide (Aldrich) to an inverse emulsion containing an aqueous phase (50 ml) dispersed in n-heptane (85/10 v/v vs. H_2O; Panreac), and using Triton X-100 (variable quantity; Aldrich) as surfactant, in 1-hexanol (105/100 v/v vs. surfactant; Aldrich). The introduction of iron and sulfur was made by adding $Fe(NO_3)_3$ (Aldrich) and $(NH_4)_2SO_4$ in the aqueous part of microemulsion. The final content of Fe was 1.5% measured as $Ti_{0.985}Fe_{0.015}O_{1.992}$. The sulfur content varied from 1% to 20% S/Ti molar ratio. The resulting mixture was vigorously stirred for 24 h, centrifuged, decanted, thoroughly rinsed under stirring with methanol in order to eliminate any portion from the organic and surfactant media, and dried at 110 °C for 24 h. The dried precipitates were calcined in air at 600 °C for 2 h using a ramp of 1 °C min^{-1}. Reference systems, single Fe-doped or S-doped TiO_2 materials, were also synthesized using the same procedure. Sample labels are: FeT for single 1.5% Fe-doped TiO_2, TS*x* for sulfur treated TiO_2 and FeTS*x* for Fe,S co-doped TiO_2 samples (where *x* is the % S/Ti molar ratio of sulfur initial concentration (1–20%)).

2.2. Characterization techniques

The composition of the catalysts was analyzed by using inductively coupled plasma and atomic absorption (ICP-AAS). BET surface area and porosity measurements were carried out by N_2 adsorption at 77 K using a Micromeritics 2010 instrument. XRD patterns were recorded in the range $10° < 2\theta < 120°$ using 0.02° steps, using a Siemens D-501 diffractometer with Ni filter and graphite monochromator with a Cu K_a X-ray source. UV–vis diffuse reflectance spectroscopy experiments were performed with a Shimadzu UV2100 apparatus with a nominal resolution of ca. 1 nm using $BaSO_4$ as reference. Diffuse Reflectance Infrared Fourier Transform Spectra (DRIFTS) were taken in a Bruker Equinox 55 FTIR spectrometer fitted with an MCT detector. The DRIFTS cell (Harrick) was fitted with CaF_2 windows and a heating cartridge that allowed samples to be heated up to 600 °C. Samples of ca. 60 mg were dehydrated at 600 °C under synthetic air (20% O_2 in He). The spectra were consisted of 50 accumulations with a total of 1 min acquisition time using a 4 cm^{-1} resolution and taken at 600 °C.

XAFS was performed at the bending magnet beamline BM23 in the European Synchrotron Radiation Facility (ESRF, Grenoble, France). The storage ring conditions were 6 GeV and 200–150 mA. The measures were performed using a Si(1 1 1) monochomator (2.0×10^{-4} $\Delta E/E$), and Si mirrors were used to eliminate higher harmonics in the beam. Three ionization chambers are filled with optimal He/N_2 gas mixture at a total pressure of 2 bar, in order to have an absorption of 30% in I_0 and 70% in I_1 and I_2 at the Fe K-edge (7112 eV). The monochromator was calibrated with a Fe foil and we constantly monitored the spectra of such foil in transmission mode in order to account for small energy shifts (<1 eV) during the measurements. The vertical exit-slit size was fixed at 0.3 mm, and the horizontal slit size was adjusted to 2.5 mm to ensure a proper counting statistics. The pre-edge region was scanned with 0.5 eV steps. Along the edge the step size was reduced to 0.4 eV in order to obtain the adequate resolution for the X-ray absorption near edge structure (XANES). The spectra were collected simultaneously in transmission and fluorescence modes (using a 13-element Ge detector for the latter).

Table 1
Chemical analysis of the calcined catalysts using inductively coupled plasma and atomic absorption (ICP-AAS).

Catalyst	Fe (%)	S (%)	N (%)
FeT	1.45	–	–
FeTS1	1.5	0.25	–
FeTS5	1.5	0.5	–
FeTS10	1.5	0.7	0.05
FeTS20	1.5	0.75	–
TS1		0.2	–
TS5		0.4	–
TS20		0.7	0.05

2.3. Photo-catalytic experimental details

Activity and selectivity for the gas-phase photo-oxidation of toluene were tested in a continuous flow annular photoreactor [24,25] containing ca. 40 mg of photocatalyst as a thin layer coating on a pyrex tube. The corresponding amount of catalyst was suspended in 1 ml of water, painted on a pyrex tube (cut-off at ca. 290 nm) and dried at room temperature. The reacting mixture (100 ml min^{-1}) was prepared by injecting toluene (Panreac, spectroscopic grade) into a wet (ca. 75% relative humidity) 20 vol.% O_2/N_2 flow before entering at room temperature to the photoreactor, yielding an organic inlet concentration of ca. 800 ppmv. After flowing the mixture for 3–4 h in the dark (control test), the catalyst was irradiated by four lamps symmetrically positioned outside the photoreactor. The photocatalytic tests were performed under a radiation spectrum simulating sunlight (Philips TL 6W/54-765) as well as under pure UV-light irradiation (Philips TL 6W/08). Reaction rates were evaluated under steady state conditions, typically achieved after 4–5 h from the beginning of irradiation. No change in activity was detected for all samples within 24 h after reaching steady state conditions. The concentration of reactants and products was analyzed using an on-line gas chromatograph (Agilent GC 6890) equipped with HP-PLOT-Q/HP-Innowax columns (0.5/0.32 mm I.D. ×30 m) and TCD/FID detectors for the quantification of CO_2 and organic substances (toluene, photo-catalytic products) respectively.

3. Results and discussion

3.1. Basic characterization

ICP-AAS spectroscopy has shown that all Fe-doped TiO_2 calcined samples had the same Fe content (1.45–1.5%). In all samples the sulfur content was lower than 1%. However, small variation of the S content was observed by varying the initial concentration. Most importantly, in all S/Fe co-doped materials moderately higher levels of sulfur were consistently detected when compared to the corresponding S single-doped TiO_2 materials (Table 1). Additionally we note the essential absence of N-impurities potentially coming from some of the chemical reagents of the synthesis for all samples.

Fig. 1 shows the XRD patterns of all TiO_2 samples calcined at 600 °C. The XRD patterns of both FeTS*x* and TS*x* series were consisted with 100% anatase crystal form. Previous studies have shown that in sulfur treated TiO_2, conversion of the anatase crystal structure to the rutile form is inhibited for calcination temperatures up to 700–750 °C [26–30]. It is worth to mention that in these S-doped TiO_2 (either single- or co-doped materials) anatase is the only phase detected for calcination temperatures up to 700 °C, while in the single-doped Fe-TiO_2 (FeT) the anatase to rutile transition was observed at $T = 650$ °C (data not shown) [26]. Small changes

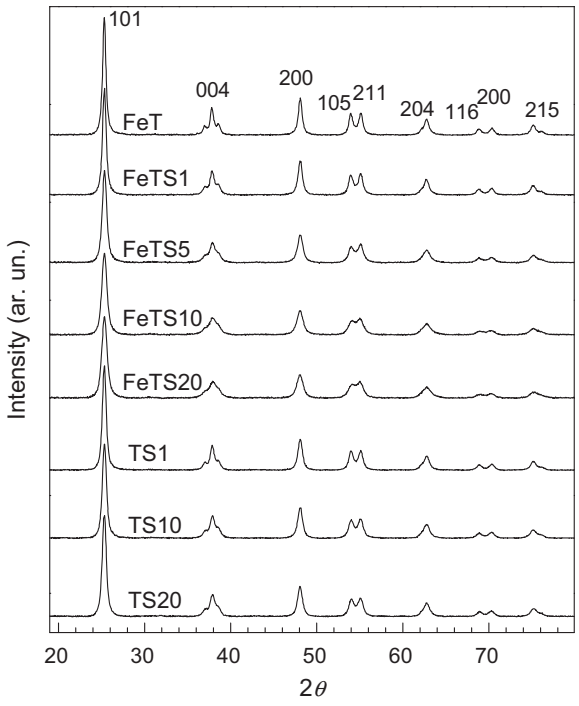

Fig. 1. XRD patterns of the FeT, FeTS*x* and TS*x* samples calcined at 600 °C.

in cell volume (increase of less than 0.4%) are detected upon the introduction of Fe into the anatase structure.

By varying the S content the XRD patterns of the FeTS*x* samples appears more affected than the corresponding to the TS*x* samples. Decreasing the S content in the FeTS*x* series resulted in a progressive narrowing of the diffraction peaks which implied an increase of the TiO_2 crystallite size and crystallinity. The crystallize sizes of anatase estimated by the Scherrer formula using the full width at half maximum (FWHM) of the most intense (1 0 1) diffraction peak are presented in Table 2. The highest crystal size was observed for the FeT sample (17.7 nm) while the smallest was for the FeTS20 (11.0 nm).

Fig. 2 shows the N_2 adsorption–desorption isotherms (Fig. 2A) and the pore size distribution plots calculated from the desorption branch of N_2 isotherm by the Barrett, Joyner and Halenda (BJH) method (Fig. 2B) of the FeT, FeTS*x* and TS*x* materials. All samples exhibited type-IV isotherms with H_2 hysteresis loop, attributed to the mesoporous structure [31,32]. The pore size distribution showed a narrow range for all samples except for the TS20, implying good homogeneity of the pores. The broader pore size distribution observed for the TS20 sample (8.4–25 nm with an average pore diameter of ~14.9 nm) is possibly caused by non-uniform pore size.

The BET surface area, total pore volume, porosity and average pore size of the investigated catalysts are listed in Table 2. First to mention is that the BET surface area of the sulfur single-doped TiO_2 was not affected by the S content. This is possibly related to the well known control of size resulting from the microemulsion method together with the relatively low temperature of calcination. As mentioned most apparent differences in presence/absence of S could be observed around or above 650 °C where the particle size growth triggers the anatase to rutile phase transformation [26]. In presence of Fe, the lower thermal stability of the anatase phase is well known and thus a more pronounced influence of S at the temperature of calcination here selected may be expected [1,5,8,9,22].

Several additional differences were detected depending on the S content. In both TS*x* and FeTS*x* series, the isotherms shown higher absorption capability at high relative pressure with increasing sulfur concentration (Fig. 2A), indicating an increase in pore volume (Table 2) [32]. In the S/Fe co-doped TiO_2 materials, increase of S content resulted in a gradual increase of the BET surface area value and pore size. This indicated that the surface area of the co-doped samples was strongly dependent on the sulfur content as has been previously observed for sulfur treated TiO_2 materials [28–30]. This may be ascribed to the fact that the increase of S content on TiO_2 limits TiO_2 anatase crystallization, i.e. disfavoring the formation of larger TiO_2 crystallites, preventing in this way the decrease of the BET surface area and shrinkage of the aggregates. This resulted in a shift to increasing pore size concomitant to the increase of the S content (Fig. 2B). This is in agreement with XRD analysis (Fig. 1) where it was shown that increase of S content resulted in lower anatase crystal size. Hence, the overall structural properties deteriorated with decreasing S content due to sintering and growth of anatase crystallites. The protection against sintering of sulfur treated TiO_2 is a well known phenomenon [28,29].

Light absorption properties were studied by UV–vis spectroscopy. Fig. 3 shows the UV–vis diffuse reflectance spectra of the S-doped TiO_2 (TS*x*) and Fe-TiO_2 (FeTS*x*) powders. The increase of the absorption at wavelength lower than 380 nm (~3.2 eV) can be assigned to the intrinsic band gap absorption of pure anatase TiO_2. In the TS*x* series a small shift of the absorption edge toward lower energies is observed for the samples TS1 and TS5 compared to TS20 (inset plot in Fig. 3, pointed with arrow). All FeTS*x* samples showed enhanced absorption in the visible region of light compared to the

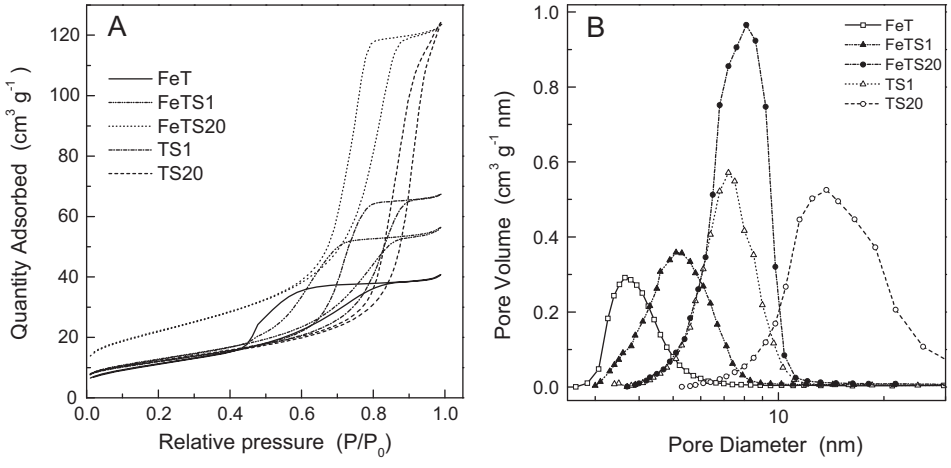

Fig. 2. N_2 adsorption–desorption isotherms (A) and pore size distribution (B) of the FeT, FeTS*x* and TS*x* samples.

Table 2
Structural characteristics of sulfur doped Fe-TiO_2 and TiO_2.

Catalyst	BET ($m^2\ g^{-1}$)	Pore volume ($ml\ g^{-1}$)[a]	Porosity (%)[b]	Pore size (nm)	Anatase crystal size (nm)[c]
FeT	41.6	0.062	19.5	4.0	17.7
FeTS1	46.1	0.086	25.1	5.2	15.7
FeTS5	55.6				13.1
FeTS10	69.6				11.3
FeTS20	77.8	0.191	42.7	7.7	11.0
TS1	42.8	0.103	28.7	7.1	15.1
TS5	47.2				13.8
TS20	42.7	0.186	42.0	14.9	14.2

[a] Total pore volume taken at relative pressure $P/P_0 = 0.98$.
[b] Porosity: estimated based on the density of anatase ($3.9\ g\ cm^{-3}$) and the pore volume determined using the adsorption branch of the N_2 isotherm at 0.98 relative pressure.
[c] Crystal size of anatase determined by XRD using Scherrer equation.

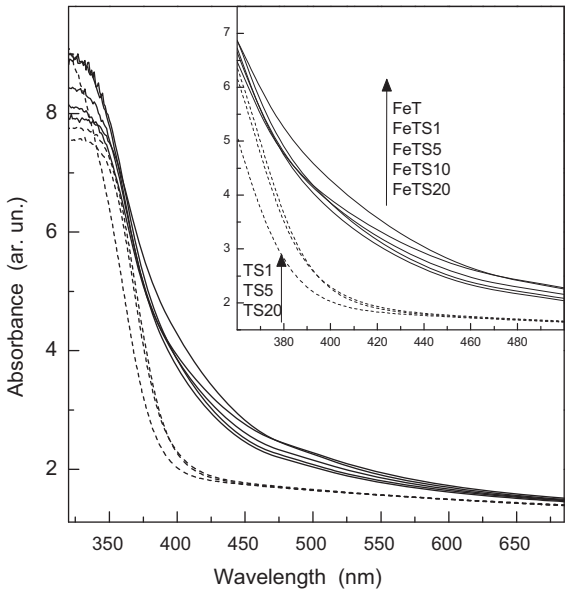

Fig. 3. Diffuse reflectance UV–vis spectra of the FeT, FeTS*x* (solid lines) and TS*x* (dashed lines) samples.

TS*x* series. This can mostly attributed to localized excitation of 3d electrons of Fe^{3+} on the TiO_2 conduction band [9,33]. Among the FeTS*x* samples, minor differences were observed. The absorbance in the visible region was slightly increased with decreasing S content (pointed with the arrow in the inset plot, Fig. 3).

3.2. S and Fe characterization

The presence of S-containing species at the surface of TiO_2 was investigated using DRIFT spectroscopy. Fig. 4 presents DRIFT spectra of different regions of the TS*x* and FeTS*x* series. In the low wavelength counterpart (Fig. 4A) the presence of a doublet at 1370–1350 and 1290–1275 cm^{-1} in the samples with S content higher than 5% may be assigned to S=O and S—O stretching vibrations respectively. These are typical ascribed to bidentate sulfate groups [34,35]. These bands were not observed for the FeT and TS1 samples. The effect of SO_4^{2-} on the acidity/basicity of TiO_2 materials it is a well established phenomenon. It has been reported that the band near 1400 cm^{-1} is an indication of higher acidity in TiO_2 materials [36]. Carbonates bands at ca. 1600–1550 cm^{-1} are also observed in Fig. 4 but those are not relevant for the present study.

Sulfur also affected drastically the high wavelength part of the DRIFT spectra. Peaks in this region (>3450 cm^{-1}) are assigned to isolated OH species (Fig. 4B) [37–40]. A first important observation is the significant decrease of the OH peak intensity for the materials with S-content ≥10%. This clearly indicates that the presence of sulfur affects the formation of isolated OH species on TiO_2 surface [26]. This effect of sulfur on the OH infrared peak intensity has been previously reported for ZrO_2 [41].

Furthermore, differences were observed on the relative intensities of the peaks at 3660–3665 and 3705–3715 cm^{-1} assigned to isolated OH-groups located on anatase (1 0 1)-type and (1 0 0)-type terminated local environments respectively [38–40]. High level S-doped TS*x* and FeTS*x* samples (i.e. $S \geq 10\%$) showed no band at (1 0 0)-surface and a very weak band at (1 0 1)-surface, in accordance with our recent detailed work [26]. This might indicate that

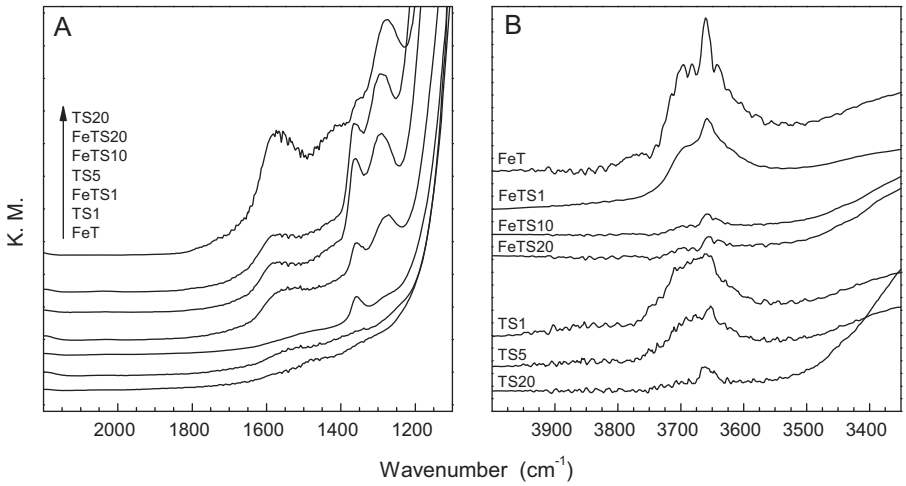

Fig. 4. DRIFT spectra of the titania catalysts taken at 600 °C under dry air.

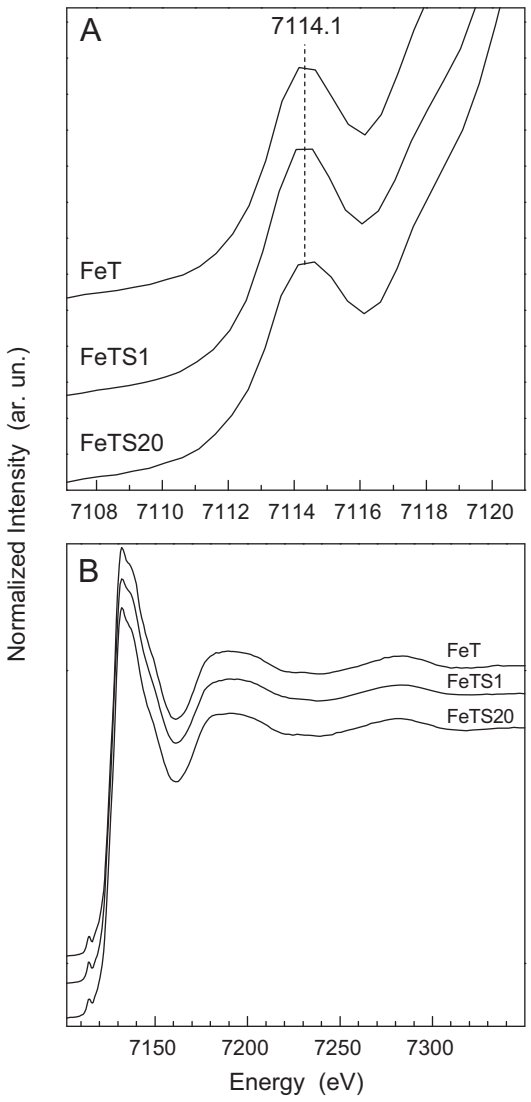

Fig. 5. Normalized Fe K-edge in the: (A) pre-edge region and (B) XANES region of FeT and FeTS*x* samples.

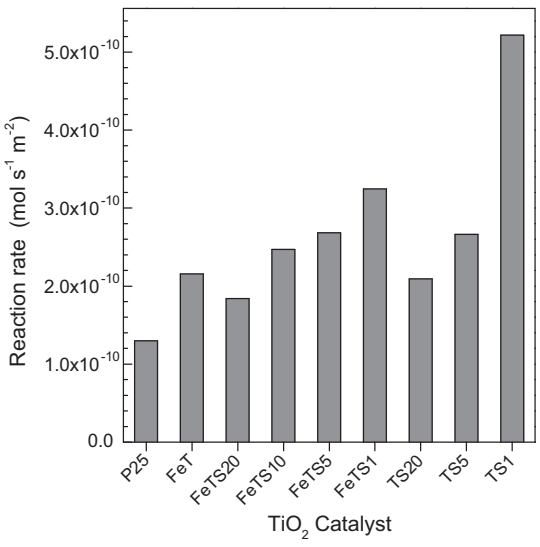

Fig. 6. Toluene photo-oxidation under sunlight irradiation (reaction rates, mol s^{-1} m^{-2}).

sulfur species preferentially anchored to (1 0 0)- rather to (1 0 1)-surfaces.

XAFS was applied to study the Fe properties on the TiO_2 catalysts. Fig. 5 shows the normalized pre-edge spectra of the FeT and FeTS*x* series taken at the Fe–K edge. Pre-edge spectra features depend on both the oxidation state and the geometry of the iron coordination [42] and were used to extract important information regarding the local symmetry characteristics of iron and its oxidation state. The energy position of the pre-edge centroid of all samples (~7114.1 eV, Table 3) is characteristic of Fe^{3+} centers (1s → p/d transition) [42–44]. The identical edge position of the Fe-doped TiO_2 samples with that of the reference hematite verified the similar oxidation (+3) state of iron on the TiO_2 samples (data not shown).

Table 3
1s3d pre-edge (Fe K-edge) characteristics of FeT and FeTS*x* samples.

Sample	Centroid position (eV)	Total area
FeT	7114.1	0.102
FeTS1	7114.05	0.100
FeTS20	7114.1	0.092

From the peak intensity the geometry around Fe^{3+} can be deduced. The total intensity (integrated area) of the pre-edge transition (see Table 3) indicated that all spectra are typical of a slightly distorted octahedral local symmetry [42,45]. Finally, based on the pre-edge spectra in Fig. 5 it is concluded that all samples are characterized by a single iron chemical species with no significant variation in local geometry and oxidation state with varying S content. This is supported by the full XANES spectra shown in Fig. 5B were no variation was detected with increasing sulfur content. It is particularly important to note that, due to the relatively low Fe content of the FeT and FeTS*x* samples, hypothetical differences among samples related to Fe surface concentration differences must be easily detected in the pre-edge analysis as changes in the coordination geometry and thus can be safely discarded. Therefore, these results indicate that sulfur does not affect the local symmetry of iron in the FeTS*x* samples, yielding rather similar Fe species in terms of structural and electronic properties.

3.3. Photocatalytic activity in toluene oxidation

Fig. 6 shows steady state reaction rates for the gas-phase photo-oxidation of toluene by the FeTS*x* and TS*x* series under artificial sunlight irradiation taking into account the different BET surface area of the samples. For comparison, the photocatalytic results obtained for the commercial reference TiO_2 Degussa P-25 is also included. Fig. 7 shows results for selected samples in similar conditions to those reported in Fig. 6 but using UV excitation. The only gaseous products detected during toluene photo-oxidation under the experimental conditions of the present study were CO_2 and benzaldehyde. The selectivity toward benzaldehyde production is presented in Fig. 8.

Under both UV and sunlight irradiation, all synthesized sulfur single or co-doped catalysts showed larger catalytic activity compared to the commercial titania, P25. Catalytic tests carried out in the dark confirmed that the measured activities were fully attributable to photo-induced processes. Note also that we carried out a gas-phase photoelimination reaction and some complex phenomena occurring with Fe-doped TiO_2 materials (e.g. iron lixiviation and readsorption from or to the solid phase; homogeneous contribution to photo-activity) in liquid phase reactions do not take place.

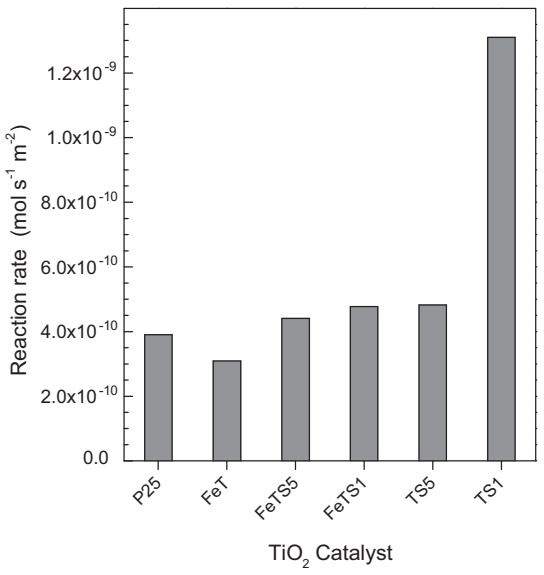

Fig. 7. Toluene photo-oxidation under UV-light irradiation (reaction rates mol s^{-1} m^{-2}).

Comparison of Figs. 6 and 7 indicates that main trends are similar and thus independent of the excitation wavelength, indicating that surface rather than electronic effects are mainly responsible for the activity behavior presented. As clearly shown by XANES, Fe structural and electronic characteristics are constant through the series of samples and thus differences in S-containing and/or OH species may be of significance to interpret photo-activity results.

Focusing first on S-containing entities, toluene photo-excitation appears to be favored at low S surface but seems clearly detrimental for high levels [46,47]. This suggests that it may be a turning point where a beneficial/detrimental effect on photo-activity can be observed with respect to the reference in a series where the S content varies. In the FeTS*x* case, we observed such point between the FeTS5 and FeTS10 samples if compared with the FeT reference system. At low S levels the acidity of the sample is clearly enhanced and this typically promotes activity [27,28,46,47]. Although not a surface property, the improved crystallinity and lower recombination rates displayed by S-stabilized high surface area has been also mentioned in this context [23,27,28]. At higher sulfur levels the interpretation is not universal but here we may provide evidence that sulfur in fact plays a second, this time negative role through its influence in the OH species.

As well known, OH species plays a capital role in pollutant photo-elimination reactions [2,48–51] and particularly in the case of toluene [25,52,53]. Fig. 4 shows that sulfur presence at TiO_2 surfaces is strongly affected by the presence/absence of Fe at the sample. In the presence of Fe, sulfur surface quantity seems to grow significantly at low levels of the anion, and thus we may speculate that the low activity of the FeTS*x* samples compared with the corresponding TS*x* references may be ascribed to detrimental effects on the OH species. As previously mentioned, we showed that the S species particularly affects the OH species at (1 0 0)/(0 0 1) surfaces. Such surfaces are currently pointed out as those having the most active centers and thus relatively small variations in their OH population may be highly significant in terms of activity reduction [5].

Summarizing, sulfur presence would implicate two opposite effects on photo-catalytic elimination of toluene. These effects are surface-related ones and thus relatively invariant with respect to the wavelength of the excitation source. Fe seems to modestly promote the sulfur negative influence of photo-activity through elimination of OH species in the highly active (1 0 0)/(0 0 1) anatase surface and thus may indicate that a highly positive, cooperative Fe–S effect can be only observed for relatively low S contents in FeTS*x* samples if compared with S-alone TiO_2 samples. In spite of this, here we observed an enhanced activity in the FeTS*x* series for $x = 1$, 5, and 10 with respect to the FeT reference, although the enhancement factor significantly decreases with S content.

Important differences in terms of reaction selectivity were also detected among the co-doped and single-doped materials (Fig. 8). We first note that the high humidity levels here used favor the stability of the catalysts (e.g. we presented pseudo-steady state measurements) but also typically favor partial vs. total oxidation products [53–55]. Partial (e.g. benzaldehyde) vs. total (e.g. CO_2) oxidation yield ratio was increased with increasing sulfur content either in Fe-TiO_2 or pure TiO_2 materials. This trend was observed under both sunlight and UV-light irradiation (Fig. 8). Catalysts FeTS20 and TS20 showed selectivity higher than 90% toward benzaldehyde formation under sunlight irradiation. Under UV-light irradiation, catalyst TS5 showed 93% selectivity toward benzaldehyde formation. This selectivity values are among the highest reported in the literature [19,56,57]. The selectivity can be related to differences in morphology, surface structure/modification and surface charge, affecting adsorption of organic substrates on the surface of TiO_2, as well as on the exposed anatase facets and particularly on OH-related surface characteristics [18,51,58–61]. As mentioned, several studies reported the importance of OH radicals on the photo-oxidation of toluene and, more importantly, the presence of two reaction pathways in the photo-catalytic mechanism related to the initial (or close to initial) radical attack to either

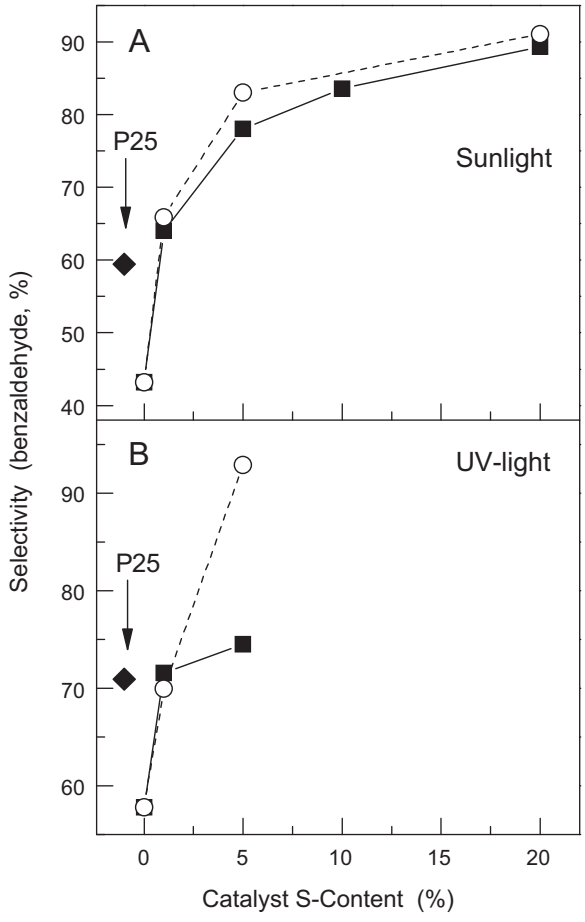

Fig. 8. Selectivity toward benzaldehyde production based on the catalyst' sulfur content under sun-light (A) and UV-light irradiation (B). Titania sample characteristics: (♦) Degussa P25; (—■—) FeTS*x* catalysts; (—○—) TS*x* catalysts.

the methyl or benzyl moieties [25,56,62]. These can be related to differences on toluene interaction with anatase which may be affected by the characteristics of the OH adsorption sites on the surface [19,58,63] and would thus drive to different oxidation products. Alternatively, the presence of S-containing species may affect the hydrophilic/hydrophobic character of TiO_2 surface and hence the adsorption of toluene on the hydrophobic sites of TiO_2. This would result in differences in catalytic selectivity through the so-call mechanism "stick-and-live", since toluene is more hydrophobic than benzaldehyde. Further studies are however required to fully interpret the selectivity of toluene photo-oxidation.

4. Conclusions

A series of sulfur and iron(III) single- and co-doped anatase titania samples were synthesized and evaluated in toluene photooxidation under UV and sunlight irradiation conditions. XAFS has shown that Fe oxidation state and local geometry was not affected by the presence of S. However, the presence of S affected significantly the surface characteristics of TiO_2 as evidenced by DRIFTS spectroscopy (isolated OH-species), as well as the structural characteristics (i.e. porosity, crystal size). Furthermore, S induced changed in both photo-activity and selectivity. The photo-activity decreases with the S content and this was attributed to the elimination of OH species in the highly active (1 0 0) anatase surface at high levels of S dopant. Low levels of S content (i.e. $\leq$10%) increased the photo-activity of the co-doped catalyst compared to the reference single doped Fe-TiO_2. In addition, the single S-doped and co-doped S/Fe-TiO_2 catalysts showed high selectivity (>90%) toward partial oxidation of toluene (benzaldehyde production). In the present samples, the data show that surface rather than electronic effects are mainly responsible for the photocatalytic activity and selectivity observed for the single- (S) and co-doped (S/Fe) catalysts. Optimization of the surface properties appears thus mandatory to render a catalyst with high photo-activity and selectivity.

Acknowledgements

Financial support by CICYT project CTQ2010-14872/BQU is fully appreciated. K.C.C. thank the Marie Curie program (action FP7-PEOPLE-2009-IEF-253445) for a Post-doctoral Fellowship. Dr. S. Pascarelli is fully thanked for the provision of beamtime at BM23 of ESRF. Dr. M.A. Newton is also thanked for some discussions concerning the experiments.

References

[1] M. Fernández-García, A. Martínez-Arias, J.C. Hanson, J.A. Rodriguez, Chem. Rev. 104 (2004) 4063–4104.
[2] M.R. Hoffmann, S.T. Martin, W. Choi, D.W. Bahnemann, Chem. Rev. 95 (1995) 69–96.
[3] A.L. Linsebigler, G. Lu, J.T. Yates Jr., Chem. Rev. 95 (1995) 735–758.
[4] R.I. Bickley, J.S. Lees, R.J.D. Tilley, L. Palmisano, M. Schiavello, J. Chem. Soc., Faraday Trans. 88 (1992) 377–383.
[5] A. Kubacka, M. Fernández-García, G. Colón, Chem. Rev. (2012), doi:10.1021/cr100454n.
[6] W. Wang, B. Gu, L. Liang, W.A. Hamilton, D.J. Weselowsky, J. Phys. Chem. B 108 (2004) 14789–14792.
[7] Z. Zhang, C. Wang, R. Zakaria, J.Y. Ying, J. Phys. Chem. B 102 (1998) 10871–10878.
[8] J.A. Navío, J.J. Testa, P. Djedjeian, J.R. Padrón, D. Rodríguez, M.I. Litter, Appl. Catal. A: Gen. 178 (1999) 191–203.
[9] C. Adan, A. Bahamonde, M. Fernández-García, A. Martínez-Arias, Appl. Catal. B: Environ. 72 (2007) 11–17.
[10] J. Yu, Q. Xiang, M. Zhou, Appl. Catal. B: Environ. 90 (2009) 595–602.
[11] C. Wang, C. Böttcher, D.W. Bahnemann, J.K. Dohrmann, J. Mater. Chem. 13 (2003) 2322–2329.
[12] M.I. Litter, J.A. Navío, J. Photochem. Photobiol. A: Chem. 98 (1996) 171–181.
[13] T. Ohno, M. Akiyoshi, T. Umebayashi, K. Asai, T. Mitsui, M. Matsumura, Appl. Catal. A: Gen. 265 (2004) 115–121.
[14] C. Han, M. Pelaez, V. Likodimos, A.G. Kontos, P. Falaras, K. O'Shea, D.D. Dionysiou, Appl. Catal. B: Environ. 107 (2011) 77–87.
[15] J.C. Yu, W. Ho, J. Yu, H. Yip, P.K. Wong, J. Zhao, Environ. Sci. Technol. 39 (2005) 1175–1179.
[16] T. Umebayashi, T. Yamaki, S. Tanala, K. Asai, Chem. Lett. 32 (2003) 330–331.
[17] Q. Li, R. Xie, E.A. Mintz, J.K. Shang, J. Am. Ceram. Soc. 90 (2007) 3863–3868.
[18] A. Kubacka, B. Bachiller-Baeza, G. Colón, M. Fernández-García, Appl. Catal. B: Environ. 93 (2010) 274–281.
[19] A. Kubacka, B. Bachiller-Baeza, G. Colón, M. Fernández-García, Appl. Catal. B: Environ. 95 (2010) 238–244.
[20] A. Kubacka, B. Bachiller-Baeza, G. Colón, M. Fernández-García, J. Phys. Chem. C 113 (2009) 8553–8555.
[21] B. Tryba, J. Hazard. Mater. 151 (2008) 623–627.
[22] T. Ohno, Z. Miyamoto, K. Nishijima, H. Kanemitsu, F. Xueyuan, Appl. Catal. A: Gen. 302 (2006) 62–68.
[23] V. Menendez-Flores, D.W. Bahnemann, T. Ohno, Appl. Catal. B: Environ. 103 (2011) 99–108.
[24] A.J. Maira, K.L. Yeung, J. Soria, J.M. Coronado, C. Belver, C.Y. Lee, V. Augugliaro, Appl. Catal. B: Environ. 29 (2001) 327–336.
[25] A. Fuerte, M.D. Hernandez-Alonso, A.J. Maira, A. Martínez-Arias, M. Fernández-García, J.C. Conesa, J. Soria, G. Munuera, J. Catal. 212 (2002) 1–9.
[26] K.C. Christoforidis, A. Iglesias-Juez, S.J.A., Figueroa, M.A., Newton, M. Di Michiel, M. Fernández-García, submitted.
[27] G. Colón, M.C. Hidalgo, J.A. Navío, Appl. Catal. B: Environ. 45 (2003) 39–50.
[28] G. Colón, M.C. Hidalgo, G. Munuera, I. Ferino, M.G. Cutrufello, J.A. Navío, Appl. Catal. B: Environ. 63 (2006) 45–59.
[29] M.C. Hidalgo, M. Maicu, J.A. Navío, G. Colón, J. Phys. Chem. C 113 (2009) 12840–12847.
[30] P. Periyat, S.C. Pillai, D.E. McCormack, J. Colreavy, S.J. Hinder, J. Phys. Chem. C 112 (2008) 7644–7652.
[31] J. Yu, Y. Su, B. Cheng, Adv. Funct. Mater. 17 (2007) 1984–1990.
[32] J. Yu, S. Liu, H. Yu, J. Catal. 249 (2007) 59–66.
[33] J. Zhu, F. Chen, J. Zhang, H. Chen, M. Anpo, J. Photochem. Photobiol. A 180 (2006) 196–204.
[34] K.J.A. Raj, B. Viswanathan, Appl. Mater. Interface 1 (2009) 2462–2469.
[35] R. Gomeza, T. Lopez, E. Ortiz-Islas, J. Navarrete, E. Sanchez, F. Tzompanztzi, X. Bokhimi, J. Mol. Catal. A: Chem. 193 (2003) 217–226.
[36] J. Xu, J. Li, W. Dai, Y. Cao, H. Li, K. Fan, Appl. Catal. B: Environ. 79 (2008) 72–80.
[37] M. Fernández-García, X. Wang, C. Belver, J.C. Hanson, J.A. Rodriguez, J. Phys. Chem. C 111 (2007) 674–682.
[38] S. Dzwigaj, C. Arrouvel, M. Breysse, C. Geantet, S. Inoue, H. Toulhoat, P. Raybaud, J. Catal. 236 (2005) 245–250.
[39] M. Digne, P. Sautet, P. Raybaud, P. Euzen, H. Touthoat, J. Catal. 211 (2002) 1–5.
[40] M. Digne, P. Sautet, P. Raybaud, P. Euzen, H. Touthoat, J. Catal. 226 (2004) 54–68.
[41] V. Indovina, M.C. Campa, F. Pepe, D. Pietrogiacomi, S. Tuti, Appl. Catal. B Environ. 60 (2005) 23–31.
[42] M. Fernández-García, Catal. Rev. 44 (2002) 59–121.
[43] F. Farges, Phys. Chem. Miner. 28 (2001) 619–629.
[44] C. Belver, M.A. Vicente, A. Martínez-Arias, M. Fernández-García, Appl. Catal. B: Environ. 50 (2004) 227–234.
[45] A.A. Battiston, J.H. Bitter, F.M.F. de Groot, A.R. Overweg, O. Stephan, J.A. van Bokhoven, P.J. Kooyman, C. van der Spek, G. Vanko, D.C. Koningsberger, J. Catal. 213 (2003) 251–271.
[46] D.S. Muggli, L. Ding, Appl. Catal. B: Environ. 32 (2001) 181–188.
[47] E. Barraud, F. Bosc, N. Keller, V. Keller, Chem. Lett. 34 (2005) 336–341.
[48] S.H. Szczepankiewicz, A.J. Colussi, M.R. Hoffmann, J. Phys. Chem. B 104 (2000) 9842–9850.
[49] R. Wang, N. Sakai, A. Fujishima, T. Watanabe, K. Hashimoto, J. Phys. Chem. B 103 (1999) 2188–2194.
[50] V.R. de Mendonca, C. Ribeiro, Appl. Catal. B: Environ. 105 (2011) 298–305.
[51] G. Palmisano, E. Garcia-Lopez, G. Marchi, V. Loddo, S. Yurdakal, V. Augugliaro, L. Palmisano, Chem. Commun. 46 (2010) 7074–7089.
[52] M. Sleirman, P. Conchon, C. Ferronato, J.M. Chovelon, Appl. Catal. B: Environ. 86 (2009) 159–165.
[53] J. Mo, Y. Zhang, Q. Xu, Y. Zhu, J.J. Lamson, R. Zhao, Appl. Catal. B: Environ. 89 (2009) 570–576.
[54] G. Colón, M. Maicu, M.C. Hidalgo, J.A. Navío, A. Kubacka, M. Fernández-García, J. Mol. Catal. A: Chem. 320 (2010) 14–18.
[55] C. Akly, P.A. Chadik, D.W. Mazyck, Appl. Catal. B: Environ. 99 (2010) 329–335.
[56] A. Maldotti, A. Molinari, R. Amadelli, Chem. Rev. 102 (2002) 3811–3836.
[57] S. Yurkadal, G. Palmisano, V. Loddo, V. Augugliaro, L. Palmisano, J. Am. Chem. Soc. 130 (2008) 1568–1569.
[58] G. Martra, Appl. Catal. A: Gen. 200 (2000) 275–285.
[59] Y. Shiraishi, N. Saito, T. Hirai, J. Am. Chem. Soc. 127 (2005) 12820–12822.
[60] S. Liu, J. Yu, M. Jaroniec, J. Am. Chem. Soc. 132 (2010) 11914–11916.
[61] Q. Xiang, J. Yu, M. Jaroniec, Chem. Commun. 47 (2011) 4532–4534.
[62] Y. Feng, L. Li, M. Ge, C. Guo, J. Wang, L. Liu, ACS Appl. Mater. Interface 2 (2010) 3134–3140.
[63] P. Du, J.A. Moujlin, G. Mul, J. Catal. 238 (2006) 342–352.